Multisensor Plug-and-Play Navigation Based on Resilient Information Filter

Qian Meng, *Member, IEEE*, Chang Su, Yingying Jiang, *Graduate Student Member, IEEE*, Weisong Wen, *Member, IEEE*, and Xiaolin Meng

***Abstract*—To improve the positioning accuracy and resilience of the multisensor integration, a resilient plug-and-play navigation method based on information filter (IF) is proposed in this article. As the dual form of Kalman filter (KF), IF turns the likelihood product into a sum, which can fully utilize asynchronous sensor measurements for fusion and realize plug-and-play navigation flexibly. Furthermore, a resilient factor based on the principle of chi-square test is implemented to adjust the sensor information, aiming to reduce the impact of faulty measurements under challenging scenarios. By conducting and analyzing the vehicle experiments in the urban environment, the proposed method shows better performance over traditional KF, with the root mean square (rms) error reduced from 9.13 to 3.28 m. Plug-and-play navigation achieves a 51.37% improvement in positioning accuracy by utilizing more suitable sensor measurements and propagation intervals, which can decrease the sensitivity to measurement noise and faults. The resilient factor directly addresses the faults themselves and improves the positioning performance by 26.13%, further enhancing the system's resilience and robustness to faulty information. This resilient IF method is fully validated as effective for multisensor plug-and-play navigation.**

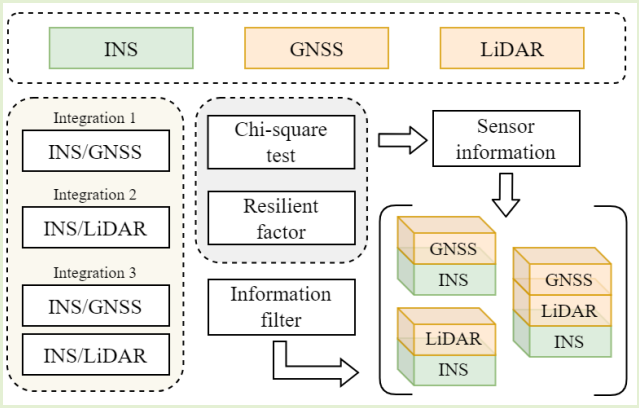

***Index Terms*—Asynchronous information, information filter (IF), multisensor integration, plug and play, resilient navigation.**

I. Introduction

WITH the rapid development in the fields of autonomous driving, autonomous aerial vehicles (AAV) navigation, wearable intelligent devices, and intelligent transportation systems [1], [2], [3], the positioning accuracy and resilience requirements of navigation systems have been increasing. Global navigation satellite system (GNSS) can achieve centimeter-level positioning accuracy in an open environment with carrier phase measurements [4]. However, in urban environments with dense buildings, tunnels, and bridges, GNSS measurements are susceptible to non-line-of-sight (NLOS) signals and multipath effect [5], [6], resulting in much lower reliability in positioning solutions. The multisensor integration approach using other navigation sensors for assisted localization is now the mainstream solution [7]. In addition to GNSS, commonly used navigation sensors include an inertial navigation system (INS), light detection and ranging (LiDAR), camera, visual INS, and so on [8]. These sensors perform differently in various scenarios [9]. For example, the errors in INS accumulate over time [10], while the performance of LiDAR is sensitive to motion distortions in urban environments [11]. Therefore, combining these sensors with each other can significantly enhance the resilience of the navigation system, which is the crucial component of resilient positioning, navigation, and timing (PNT).

Resilient PNT aims to aggregate redundant information to enhance the availability, continuity, and reliability of

Received 22 January 2025; revised 5 February 2025; accepted 7 February 2025. Date of publication 26 February 2025; date of current version 2 April 2025. This work was supported in part by the National Natural Science Foundation of China under Grant 62203111 and Grant 62388101, in part by the Aeronautical Science Foundation of China under Grant 20220008069003, in part by the Natural Science Foundation of Jiangsu Province under Grant BK20231434, and in part by Jiangsu Provincial Department of Science and Technology under Grant BM2023013. The associate editor coordinating the review of this article and approving it for publication was Prof. Jun Wang. *(Corresponding author: Qian Meng.)*

Qian Meng, Chang Su, and Xiaolin Meng are with the Key Laboratory of Micro-Inertial Instrument and Advanced Navigation Technology, Ministry of Education, School of Instrument Science and Engineering, Southeast University, Nanjing 210096, China (e-mail: qianmeng@seu.edu.cn; 220233664@seu.edu.cn; xiaolin_meng@seu.edu.cn).

Yingying Jiang is with the GEOLOC Laboratory, AME Department, Gustave Eiffel University, 44344 Nantes, France (e-mail: yingying.jiang@univ-eiffel.fr).

Weisong Wen is with the Department of Aeronautical and Aviation Engineering, Hong Kong Polytechnic University, Hong Kong (e-mail: Welson.wen@polyu.edu.hk).

Digital Object Identifier 10.1109/JSEN.2025.3540790

navigation systems, for the potential risks of relying on a single information source [12]. These risks can arise from various aspects such as environment and weather, leading to measurements of navigation sensors inevitably having faults and outliers. If these faults cannot be detected in time, the positioning performance of the navigation system will be significantly affected, which is intolerable for safety-critical services [13]. To address this problem, representative methods are proposed and studied to enhance resilient information fusion, including autonomous integrity and robust estimation [14], [15]. The former executes fault detection and exclusion (FDE), which is based on the consistency test principle and identifies the faults by constructing a test statistic [16]. For instance, extended receiver autonomous integrity monitoring (ERAIM) is based on the least squares redundancy model [17]. The latter in most cases models outliers as a random model, including M-estimation, R-estimation, and random sampling [18]. Among them, M-estimation realizes the suppression of faults by controlling the weights of each measurement through variance inflation after selecting appropriate equivalent weight functions and robust coefficients [19], [20]. Both these two methods can effectively reduce the influence of faulty measurements in the navigation system.

Resilient navigation methods based on multisensor integration have received extensive research attention. Meng and Hsu [7] construct a resilient interactive structure between different sensors, which can employ a Markov chain to dynamically update the transition information and model likelihood. Chen and Zhao [21] propose a multilevel integrity monitoring method for resilient fusion navigation. This method implements fault detection and verification of navigation sources and sensors at both the system level and sensor level. Then the observed information can be adjusted in the resilient navigation solution. To address global positioning system (GPS) outrages, [22] denoises the INS measurements and proposes a temporal dynamic attention neural network, which can predict the position increment and keep the filtering process. Gipson and Leishman [23] fuses collaboratively all-source navigation information in a resilient manner. On the basis of autonomous and resilient management of the all-source sensors framework [24], this manner utilizes stable observability monitoring as the augmentation and provides FDE and integrity monitoring in a collaborative network. In addition, a decentralized framework in multisensor systems is also a key focus now. Several studies are conducted around this topic, such as the federated filter with adaptive information sharing factor [25] and multisensor optimal data fusion method based on robust unscented Kalman filter (KF) [26].

To summarize, most of the above work is conducted using KF, which is widely used in engineering applications for its mature structure, simple computation, and numerous improvements. However, it is precisely due to the fixed structure of the KF, that the navigation system is typically based on the specific architecture of sensors and integrates them at the lowest frequency. This will bring significant costs when the system needs to change, for that the structure of measurement vector, measurement matrix, and so on must be adjusted continuously. Therefore, the navigation system cannot achieve the plug-and-play capability for heterogeneous and asynchronous navigation information [27]. For this point, the existing plug-and-play methods often concentrate on factor graph optimization (FGO), which can retain historical information and perform global optimization to improve the estimation accuracy [28]. However, FGO also has issues such as high-computational demands and latency [29], [30]. Based on the superiorities of KF mentioned above, the core work of this article aims to use the filtering theory and resilient PNT solution to implement multisensor plug-and-play navigation.

In the research of filtering solutions, an information filter (IF) is considered a substitute for the traditional KF, which functions as its dual and inverse covariance form. The performance of them is theoretically equivalent [31], and their difference mainly arises from the representation of Gaussian belief [32]. The implementation of IF can be summarized as the linear combination of contributions from different sensors. It is easy to evaluate the overall measurements from each sensor, enabling resilient adjustment of the faulty sensor in the update processing. Compared to KF, IF can better utilize asynchronous information, making it possible to achieve plug-and-play navigation. Thus, a resilient plug-and-play IF (RPIF) method is proposed to improve the positioning accuracy and resilience of the multisensor navigation system. This method is primarily motivated by maximizing the flexible use of observational information in the filter. In the proposed solution, IF can convert the fixed structure in KF into a sum form and INS is used as the state estimator for prior prediction. This method assumes that INS operates properly during the process and considers no impact of its fault on the system. Therefore, whenever the system detects asynchronous measurements, the filter simply needs to add them to this predicted information. Then the system allows each sensor and INS to be integrated separately, and a resilient factor based on the chi-square test is calculated to adjust the sensor information. Finally, INS/GNSS/LiDAR vehicle experiments are conducted and analyzed to evaluate the effectiveness of this method in urban environment.

The main contributions of this article are summarized as follows.

1) A multisensor plug-and-play navigation solution based on IF is implemented, which can make full use of the additive and subtractive structure of the IF to achieve asynchronous multisensor information fusion and flexible sensor selection.
2) A resilient IF method is proposed to enhance the resilience and continuity of multisensor navigation under challenging scenarios. The reliability of each sensor can be evaluated using the principle of the chi-square test, which results in a novel resilient factor calculated to adjust sensor information dynamically online.
3) The proposed plug-and-play navigation method based on resilient IF is validated in an urban canyon environment. The discussion of the effectiveness of the proposed method has been analyzed from the perspective of innovation, propagation interval, and positioning errors in detail.

The remainder of this article is organized as follows. In Section II, the multisensor integration model and KF is elaborately described, including corresponding equation development and parameter estimations. In Section III, the proposed method is introduced, including the derivation of parameters relevant to IF and the implementation process of the method. Section IV introduces the experimental scenario and data, and analyses the positioning results. Section V compares the differences in innovation, and discusses the reasons behind the superiority of the proposed method. Finally, Section VI gives the conclusion and future work of this article.

II. MultiSensor Integration Based on KF

In this section, the INS/GNSS/LiDAR multisensor model is set up according to [33], with the traditional KF and its corresponding equations and parameters introduced.

A. Multisensor Integration Model

The INS/GNSS/LiDAR multisensor model employs loosely coupled integration. The state vector of the model is

$$\boldsymbol{X}_k = [\,\delta\boldsymbol{\varphi} \quad \delta\boldsymbol{v} \quad \delta\boldsymbol{p} \quad \delta\boldsymbol{b_a} \quad \delta\boldsymbol{b_g}\,]^{\mathrm{T}} \tag{1}$$

where $\delta\boldsymbol{\varphi}$, $\delta\boldsymbol{v}$, and $\delta\boldsymbol{p}$ are the 3-D attitude, velocity, and position error vector in the Earth-centered, Earth-fixed (ECEF) frame, respectively. $\delta\boldsymbol{b_a}$ and $\delta\boldsymbol{b_g}$ are the 3-D accelerometer and gyro bias vector, respectively.

The state equation of the model is

$$\boldsymbol{X}_k = \boldsymbol{\Phi}_{k/k-1}\boldsymbol{X}_{k-1} + \boldsymbol{w}_k \tag{2}$$

where $\boldsymbol{w}_k$ is the noise vector which satisfies $E[\boldsymbol{w}_k] = 0$ and $E[\boldsymbol{w}_k^{\mathrm{T}}\boldsymbol{w}_k] = \boldsymbol{Q}_k$.

$\boldsymbol{\Phi}_{k/k-1}$ is the state transition matrix, defined as (3), shown at the bottom of the next page, where $[\cdot\times]$ represents the skew-symmetric matrix, τ_s is the propagation interval, $\boldsymbol{\omega}_{ie}^{e}$ is the Earth rotation rate, $\hat{\boldsymbol{C}}_b^e$ is the coordinate transformation matrix from body frame to ECEF frame, $\hat{\boldsymbol{f}}_{ib}^{b}$ is the specific force, $\hat{g}_{ib}^{e}$ calculates the acceleration due to gravity, and r_{eS}^{e} calculates the geocentric radius.

$\boldsymbol{Q}_k$ is the system noise covariance matrix

$$\boldsymbol{Q}_k = \begin{bmatrix} \boldsymbol{S}_{rg}\tau_s & \boldsymbol{0}_3 & \boldsymbol{0}_3 & \boldsymbol{0}_3 & \boldsymbol{0}_3 \\ \boldsymbol{0}_3 & \boldsymbol{S}_{ra}\tau_s & \boldsymbol{0}_3 & \boldsymbol{0}_3 & \boldsymbol{0}_3 \\ \boldsymbol{0}_3 & \boldsymbol{0}_3 & \boldsymbol{0}_3 & \boldsymbol{0}_3 & \boldsymbol{0}_3 \\ \boldsymbol{0}_3 & \boldsymbol{0}_3 & \boldsymbol{0}_3 & \boldsymbol{S}_{bad}\tau_s & \boldsymbol{0}_3 \\ \boldsymbol{0}_3 & \boldsymbol{0}_3 & \boldsymbol{0}_3 & \boldsymbol{0}_3 & \boldsymbol{S}_{bgd}\tau_s \end{bmatrix} \tag{4}$$

where $\boldsymbol{S}_{rg}$, $\boldsymbol{S}_{ra}$, $\boldsymbol{S}_{bad}$, and $\boldsymbol{S}_{bgd}$ are the power spectral density (PSD) of the gyro noise, accelerometer noise, accelerometer bias random walk, and gyro bias random walk, respectively.

The measurement equation of the multisensor model is

$$\boldsymbol{Z}_k = \boldsymbol{H}_k\boldsymbol{X}_k + \boldsymbol{v}_k \tag{5}$$

where $\boldsymbol{v}_k$ is the measurement noise vector which satisfies $E[\boldsymbol{v}_k] = 0$ and $E[\boldsymbol{v}_k^{\mathrm{T}}\boldsymbol{v}_k] = \boldsymbol{R}_k$.

$\boldsymbol{Z}_k$ is the measurement vector, defined as the difference of positioning outputs between each sensor and INS

$$\boldsymbol{Z}_k = \begin{bmatrix} \boldsymbol{p}_{\mathrm{GNSS}} - \boldsymbol{p}_{\mathrm{INS}} \\ \boldsymbol{p}_{\mathrm{LiDAR}} - \boldsymbol{p}_{\mathrm{INS}} \end{bmatrix} \tag{6}$$

where $\boldsymbol{p}_{\mathrm{INS}}$, $\boldsymbol{p}_{\mathrm{GNSS}}$, and $\boldsymbol{p}_{\mathrm{LiDAR}}$ are the 3-D positioning outputs of INS, GNSS, and LiDAR, respectively.

The $\boldsymbol{H}_k$ is the measurement matrix

$$\boldsymbol{H}_k = \begin{bmatrix} \boldsymbol{0}_{3\times6} & -\boldsymbol{I}_3 & \boldsymbol{0}_{3\times6} \\ \boldsymbol{0}_{3\times6} & -\boldsymbol{I}_3 & \boldsymbol{0}_{3\times6} \end{bmatrix} \tag{7}$$

$\boldsymbol{R}_k$ is the noise covariance matrix

$$\boldsymbol{R}_k = \begin{bmatrix} \boldsymbol{\sigma}^2_{\mathrm{GNSS}} & \boldsymbol{0}_3 \\ \boldsymbol{0}_3 & \boldsymbol{\sigma}^2_{\mathrm{LiDAR}} \end{bmatrix} \tag{8}$$

where $\boldsymbol{\sigma}^2_{\mathrm{GNSS}}$ and $\boldsymbol{\sigma}^2_{\mathrm{LiDAR}}$ are the 3-D positioning noise variances of GNSS and LiDAR.

B. Kalman Filter

The main steps of KF include state prediction and measurement update. In the first step, with the state transition matrix and system noise covariance matrix, the prior state and corresponding covariance matrix at epoch k can be predicted from the posterior state and corresponding covariance matrix at epoch $k-1$

$$\hat{\boldsymbol{X}}_{k/k-1} = \boldsymbol{\Phi}_{k/k-1}\hat{\boldsymbol{X}}_{k-1} \tag{9}$$

$$\boldsymbol{P}_{k/k-1} = \boldsymbol{\Phi}_{k/k-1}\boldsymbol{P}_{k-1}\boldsymbol{\Phi}_{k/k-1}^{\mathrm{T}} + \boldsymbol{Q}_{k-1} \tag{10}$$

where $\hat{\boldsymbol{X}}_{k/k-1}$ and $\hat{\boldsymbol{X}}_{k-1}$ are the prior state vector and posterior state vector. $\boldsymbol{P}_{k/k-1}$ and $\boldsymbol{P}_{k-1}$ are the corresponding covariance matrix of each state vector.

Then in the next step, the Kalman gain matrix is computed. Based on this, the posterior state and corresponding covariance matrix at epoch k are updated by the prior state and covariance matrix, the measurement vector, and noise covariance matrix

$$\boldsymbol{K}_k = \boldsymbol{P}_{k/k-1}\boldsymbol{H}_k^{\mathrm{T}}\left(\boldsymbol{H}_k\boldsymbol{P}_{k/k-1}\boldsymbol{H}_k^{\mathrm{T}} + \mathbf{R}_k\right)^{-1} \tag{11}$$

$$\hat{\boldsymbol{X}}_k = \hat{\boldsymbol{X}}_{k/k-1} + \boldsymbol{K}_k\left(\boldsymbol{Z}_k - \boldsymbol{H}_k\hat{\boldsymbol{X}}_{k/k-1}\right) \tag{12}$$

$$\boldsymbol{P}_k = (\boldsymbol{I} - \boldsymbol{K}_k\boldsymbol{H}_k)\boldsymbol{P}_{k/k-1} \tag{13}$$

where $\boldsymbol{K}_k$ is the Kalman gain matrix, $\boldsymbol{R}_k$ is the noise matrix, $\hat{\boldsymbol{X}}_k$ is the posterior state vector at epoch k, and $\boldsymbol{P}_k$ is the corresponding covariance matrix.

III. Plug-and-Play Navigation Method Enhanced by Resilient IF

This section derives the IF from KF and describes its superiorities for multisensor navigation. Then the resilient factor based on the principle of the chi-square test is deduced to improve the resilience and continuity of navigation under challenging scenarios.

A. IF Derived From KF

The introduction mentions that IF is the dual form of KF and the main difference between them is the representation of Gaussian belief. In KF, Gaussians are represented by moments including mean and covariance. While in IF, they are converted to the canonical form, including information matrix and information vector as follows [32]:

$$\begin{cases} \boldsymbol{\Omega} = \boldsymbol{P}^{-1} \\ \boldsymbol{\xi} = \boldsymbol{\Omega}\boldsymbol{X} \end{cases} \tag{14}$$

where $\boldsymbol{\Omega}$ is the information matrix, and the inverse of the covariance matrix. $\boldsymbol{\xi}$ is the information vector, and the product of $\boldsymbol{\Omega}$ and state vector.

Substitute (9) and (10) to (14), the prediction step of IF can be written as

$$\boldsymbol{\Omega}_{k/k-1} = \left(\boldsymbol{\Phi}_{k/k-1}\boldsymbol{\Omega}_{k-1}^{-1}\boldsymbol{\Phi}_{k/k-1}^{\mathrm{T}} + \boldsymbol{Q}_{k-1}\right)^{-1} \tag{15}$$

$$\boldsymbol{\xi}_{k/k-1} = \boldsymbol{\Omega}_{k/k-1}\left(\boldsymbol{\Phi}_{k/k-1}\boldsymbol{\Omega}_{k-1}^{-1}\boldsymbol{\xi}_{k-1}\right) \tag{16}$$

where $\boldsymbol{\Omega}_{k/k-1}$ and $\boldsymbol{\xi}_{k/k-1}$ are the prior information matrix and information vector at epoch k. $\boldsymbol{\Omega}_{k-1}$ and $\boldsymbol{\xi}_{k-1}$ are the posterior information matrix and information vector at epoch $k-1$.

Then the measurement update step can be deduced. Substitute (11) and (13) to (14), the information matrix is derived as

$$\begin{aligned}\boldsymbol{\Omega}_k = \boldsymbol{P}_k^{-1} &= \left[(\boldsymbol{I} - \boldsymbol{K}_k\boldsymbol{H}_k)\boldsymbol{\Omega}_{k/k-1}^{-1}\right]^{-1} \\ &= \left[\boldsymbol{\Omega}_{k/k-1}^{-1} - \boldsymbol{\Omega}_{k/k-1}^{-1}\boldsymbol{H}_k^{\mathrm{T}}\left(\boldsymbol{R}_k + \boldsymbol{H}_k\boldsymbol{\Omega}_{k/k-1}^{-1}\boldsymbol{H}_k^{\mathrm{T}}\right)\boldsymbol{H}_k\boldsymbol{\Omega}_{k/k-1}^{-1}\right]^{-1} \\ &= \boldsymbol{\Omega}_{k/k-1} + \boldsymbol{H}_k^{\mathrm{T}}\boldsymbol{R}_k^{-1}\boldsymbol{H}_k \end{aligned} \tag{17}$$

where $\boldsymbol{\Omega}_k$ is the posterior information matrix at epoch k and the second row is transformed to the third row by matrix inversion lemma.

The Kalman gain matrix in (11) can be expanded by the inversion lemma and substituted with the above equation as [34]

$$\begin{aligned}\boldsymbol{K}_k &= \boldsymbol{P}_{k/k-1}\left(\boldsymbol{I} - \boldsymbol{H}_k^{\mathrm{T}}\boldsymbol{R}_k^{-1}\boldsymbol{H}_k\boldsymbol{\Omega}_k^{-1}\right)\boldsymbol{H}_k^{\mathrm{T}}\boldsymbol{R}_k^{-1} \\ &= \boldsymbol{P}_{k/k-1}\left(\boldsymbol{\Omega}_k - \boldsymbol{H}_k^{\mathrm{T}}\boldsymbol{R}_k^{-1}\boldsymbol{H}_k\right)\boldsymbol{\Omega}_k^{-1}\boldsymbol{H}_k^{\mathrm{T}}\boldsymbol{R}_k^{-1} \\ &= \boldsymbol{\Omega}_k^{-1}\boldsymbol{H}_k^{\mathrm{T}}\boldsymbol{R}_k^{-1}. \end{aligned} \tag{18}$$

Information vectors can be calculated from (12) and (14)

$$\begin{aligned}\boldsymbol{\xi}_k = \boldsymbol{\Omega}_k\hat{\boldsymbol{X}}_k &= \boldsymbol{\Omega}_k\left[(\boldsymbol{I} - \boldsymbol{K}_k\boldsymbol{H}_k)\hat{\boldsymbol{X}}_{k/k-1} + \boldsymbol{K}_k\boldsymbol{Z}_k\right] \\ &= \boldsymbol{\Omega}_k\left[\boldsymbol{\Omega}_k^{-1}\left(\boldsymbol{\Omega}_k - \boldsymbol{H}_k^{\mathrm{T}}\boldsymbol{R}_k^{-1}\mathbf{H}_k\right)\hat{\boldsymbol{X}}_{k/k-1} + \boldsymbol{\Omega}_k^{-1}\boldsymbol{H}_k^{\mathrm{T}}\boldsymbol{R}_k^{-1}\boldsymbol{Z}_k\right] \\ &= \boldsymbol{\Omega}_{k/k-1}\hat{\boldsymbol{X}}_{k/k-1} + \boldsymbol{H}_k^{\mathrm{T}}\boldsymbol{R}_k^{-1}\boldsymbol{Z}_k \\ &= \boldsymbol{\xi}_{k/k-1} + \boldsymbol{H}_k^{\mathrm{T}}\boldsymbol{R}_k^{-1}\boldsymbol{Z}_k \end{aligned} \tag{19}$$

where $\boldsymbol{\xi}_k$ is the posterior information vector at epoch k. The details of derivation from KF to IF are presented above, and it can be seen that the Kalman gain matrix has been simplified and combined into (17) and (19).

B. Plug-and-Play Navigation Based on IF

Both the KF and IF are generally based on Bayes' rule for combining the prior state and measurement information. For multisensor integration, the measurements of each sensor are assumed to be conditionally independent

$$\begin{aligned}P(\boldsymbol{Z}^{\mathrm{n}}|\boldsymbol{X}) &= P(\boldsymbol{Z}^{(1)}, \boldsymbol{Z}^{(2)}, \ldots, \boldsymbol{Z}^{(\mathrm{n})}|\boldsymbol{X}) \\ &= P(\boldsymbol{Z}^{(1)}|\boldsymbol{X})P(\boldsymbol{Z}^{(2)}|\boldsymbol{X}), \ldots, P(\boldsymbol{Z}^{(\mathrm{n})}|\boldsymbol{X}) \\ &= \prod_{\mathrm{i}=1}^{\mathrm{n}} P(\boldsymbol{Z}^{(i)}|\boldsymbol{X}) \end{aligned} \tag{20}$$

where $\boldsymbol{Z}^{\mathrm{n}} = [\boldsymbol{Z}^{(1)}, \boldsymbol{Z}^{(2)}, \ldots, \boldsymbol{Z}^{(\mathrm{n})}]$ is the set of all measurements.

By combining with (20), Bayes' rule can be derived as

$$\begin{aligned}P(\boldsymbol{X}|\boldsymbol{Z}^{\mathrm{n}}) &= \frac{P(\boldsymbol{Z}^{\mathrm{n}}|\boldsymbol{X})P(\boldsymbol{X})}{P(\boldsymbol{Z}^{\mathrm{n}})} \\ &= \frac{1}{P(\boldsymbol{Z}^{\mathrm{n}})}P(\boldsymbol{X})\prod_{\mathrm{i}=1}^{\mathrm{n}} P(\boldsymbol{Z}^{(i)}|\boldsymbol{X}) \end{aligned} \tag{21}$$

where $P(\boldsymbol{X}|\boldsymbol{Z}^{\mathrm{n}})$, $P(\boldsymbol{X})$, and $P(\boldsymbol{Z}^{(i)}|\boldsymbol{X})$ are the posterior probability, prior probability, and conditional probability, respectively. $P(\boldsymbol{Z}^{\mathrm{n}})$ is used as the normalizing constant.

Correspondingly, when the measurement is fixed and $\boldsymbol{X}$ varies, $P(\boldsymbol{Z}^{(i)}|\boldsymbol{X})$ can be referred to as the likelihood, and the above equation functions as the independent likelihood pool [35]. The prior of each information source is the same. Then the posterior is proportional to the product of this prior and each independent likelihood.

While for IF, it is essential a log-likelihood form of Bayes' rule, and the product of each independent likelihood can be turned into a sum [36]. Thus, (17) and (19) are converted to the sum of the prediction and information contribution of each sensor measurement in the update step

$$\boldsymbol{\Omega}_k = \boldsymbol{\Omega}_{k/k-1} + \sum_{i=1}^{\mathrm{n}} \boldsymbol{H}_k^{(i)^{\mathrm{T}}}\boldsymbol{R}_k^{(i)^{-1}}\boldsymbol{H}_k^{(i)} \tag{22}$$

$$\boldsymbol{\xi}_k = \boldsymbol{\xi}_{k/k-1} + \sum_{i=1}^{\mathrm{n}} \boldsymbol{H}_k^{(i)^{\mathrm{T}}}\boldsymbol{R}_k^{(i)^{-1}}\boldsymbol{Z}_k^{(i)} \tag{23}$$

where $\boldsymbol{Z}_k^{(i)}$, $\boldsymbol{H}_k^{(i)}$ and $\boldsymbol{R}_k^{(i)}$ are the measurement vector, measurement matrix, and noise covariance matrix of the ith sensor, respectively.

Then, the functional procedure and comparison between KF and IF is shown in Fig. 1. Different from definitions in KF, the measurement vector in IF is

$$\boldsymbol{Z}_k^{(\mathrm{i})} = \left[\boldsymbol{p}_{(i)} - \boldsymbol{p}_{\mathrm{INS}}\right]. \tag{24}$$

The corresponding measurement matrix and noise covariance matrix are

$$\boldsymbol{H}_k^{(i)} = \begin{bmatrix}\mathbf{0}_{3\times6} & -\boldsymbol{I}_3 & \mathbf{0}_{3\times6}\end{bmatrix} \tag{25}$$

$$\boldsymbol{R}_k^{(i)} = \begin{bmatrix}\boldsymbol{\sigma}_{(i)}^2 & 0 & 0 \\ 0 & \boldsymbol{\sigma}_{(i)}^2 & 0 \\ 0 & 0 & \boldsymbol{\sigma}_{(i)}^2\end{bmatrix} \tag{26}$$

$$\boldsymbol{\Phi}_{k/k-1} = \begin{bmatrix} \boldsymbol{I}_3 - \left[\boldsymbol{\omega}_{ie}^e\times\right]\tau_s & 0_3 & 0_3 & 0_3 & \hat{\boldsymbol{C}}_b^e\tau_s \\ \left[-\hat{\boldsymbol{C}}_b^e\hat{\boldsymbol{f}}_{ib}^b\times\right]\tau_s & \boldsymbol{I}_3 - 2\left[\boldsymbol{\omega}_{ie}^e\times\right]\tau_s & -\dfrac{2\hat{\boldsymbol{g}}_{ib}^e}{r_{eS}^e(\hat{L}_b)}\dfrac{\hat{\boldsymbol{p}}_{eb}^{e\ \mathrm{T}}}{\left|\hat{\boldsymbol{p}}_{eb}^e\right|}\tau_s & \hat{\boldsymbol{C}}_b^e\tau_s & 0_3 \\ 0_3 & \boldsymbol{I}_3\tau_s & \boldsymbol{I}_3 & 0_3 & 0_3 \\ 0_3 & 0_3 & 0_3 & \boldsymbol{I}_3 & 0_3 \\ 0_3 & 0_3 & 0_3 & 0_3 & \boldsymbol{I}_3 \end{bmatrix}. \tag{3}$$

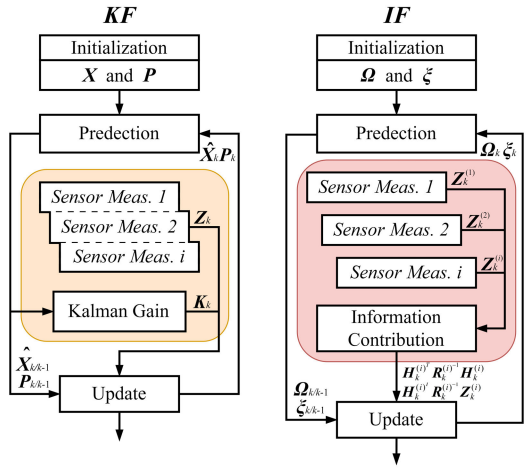

Fig. 1. Functional procedure and comparison between KF and IF.

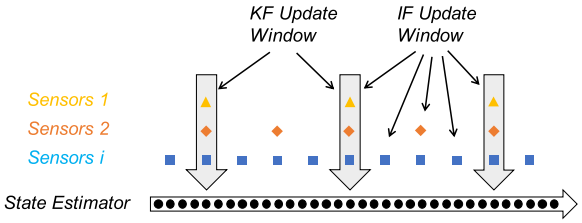

Fig. 2. Comparison between KF update window and IF update window.

where $\boldsymbol{p}_{(i)}$ and $\boldsymbol{\sigma}^2_{(i)}$ are the 3-D positioning outputs and positioning noise variance of the ith sensor.

The superiorities of IF for multisensor navigation can be explained in the following four aspects.

1) Plug and Play: The comparison of the update window between two filters is shown in Fig. 2, where different shapes represent asynchronous sensor measurements and each column means a measurement combination. In KF, this combination is relatively fixed, and adjusting parameters to accommodate each combination will undoubtedly increase the cost. While in IF, different sensors can be independent for their sum form and their combination is no longer fixed. Once one sensor is available, it can be simply added to the sum of information contribution. Therefore, IF is pretty suitable for all-source plug-and-play navigation.

2) Dimension and Computation: For multisensor integration, the dimension of the measurement vector is often very big in KF, which results in a big dimension of the measurement matrix and filter gain. It is clear that the update process of IF is much simpler. There's no need to calculate the filter gain. Even though IF involves many matrix inversions, the meticulous research about the calculation burden between two filters still verified that the IF is faster when the measurement vector dimension is 1.65 times bigger than the state vector dimension for time-varying systems and 0.75 times bigger than the latter one for time-invariant systems [31]. This can provide more advantages when dealing with more complex multisensor integration.

3) Initialization: For navigation in a challenging environment, initialization is often a problem for KF. Special provisions have to be made to handle the problem in KF. While for IF, it is easy to set the information estimation as zero information.

4) Fault Exclusion: The implementation of the fault exclusion function in KF is still a research point. No matter the parallel subfilters method (also known as solution separation) or partial update formulation will add the process complexity [37], [38]. The sum form of IF makes it easy to isolate and exclude the faulty sensor in the update process [39].

C. Resilient Factor Based on Chi-Square Test

To improve the resilience and continuity of navigation under challenging scenarios, it is essential to promptly detect and exclude the outliers in the observation. By utilizing the principle of chi-square test based on innovation, the reliability of each single sensor can be evaluated. Then in the last part, IF is concluded as suitable for fault exclusion due to its special structure. Similarly, this article calculates the resilient factor to adjust sensor information instead of directly excluding it, allowing for the retention of reliable information.

From (22) and (23), it can be seen that $\boldsymbol{\Omega}_{k/k-1}$ and $\boldsymbol{\xi}_{k/k-1}$ are the prior information of the system. While one sensor measurement is received in the process, its information of $\boldsymbol{H}_k^{(i)^{\mathrm{T}}}\boldsymbol{R}_k^{(i)^{-1}}\boldsymbol{H}_k^{(i)}$ and $\boldsymbol{H}_k^{(i)^{\mathrm{T}}}\boldsymbol{R}_k^{(i)^{-1}}\boldsymbol{Z}_k^{(i)}$ are integrated into the information matrix and information vector. Thus, a resilient factor can be used to adjust the weight of the sensor information

$$\boldsymbol{\Omega}_k = \boldsymbol{\Omega}_{k/k-1} + \sum_{i=1}^{\mathrm{n}} \lambda_k^{(i)} \boldsymbol{H}_k^{(i)^{\mathrm{T}}} \boldsymbol{R}_k^{(i)^{-1}} \boldsymbol{H}_k^{(i)} \tag{27}$$

$$\boldsymbol{\xi}_k = \boldsymbol{\xi}_{k/k-1} + \sum_{i=1}^{\mathrm{n}} \lambda_k^{(i)} \boldsymbol{H}_k^{(i)^{\mathrm{T}}} \boldsymbol{R}_k^{(i)^{-1}} \boldsymbol{Z}_k^{(i)} \tag{28}$$

where $\lambda_k^{(i)}$ is the resilient factor of the ith sensor and estimated by the principle of chi-square test.

Before constructing the test statistic, it is necessary to define the measurement innovation and its covariance of the ith sensor

$$\boldsymbol{\gamma}_k^{(i)} = \boldsymbol{Z}_k^{(i)} - \boldsymbol{H}_k^{(i)} \hat{\boldsymbol{X}}_{k/k-1} \tag{29}$$

$$\boldsymbol{S}_k^{(i)} = \boldsymbol{H}_k^{(i)} \boldsymbol{\Omega}_{k/k-1}^{-1} \boldsymbol{H}_k^{(i)^{\mathrm{T}}} + \boldsymbol{R}_k^{(i)}. \tag{30}$$

From the statistical properties of the innovation, it is known that when the measurement is under fault-free conditions, $\boldsymbol{\gamma}_k^{(i)}$ follows a Gaussian distribution with a mean zero, which is proposed as the null hypothesis $H_0 : \boldsymbol{\gamma}_k^{(i)} \sim N(0, \boldsymbol{S}_k^{(i)})$. However, if there are outliers in the measurement, the mean of the innovation is no longer zero, and this situation is defined as the alternative hypothesis $H_1 : \boldsymbol{\gamma}_k^{(i)} \sim N(\mu, \boldsymbol{S}_k^{(i)})$.

The test statistic can be calculated as [40]

$$q_k^{(i)} = \boldsymbol{\gamma}_k^{(i)^{\mathrm{T}}} \boldsymbol{S}_k^{(i)^{-1}} \boldsymbol{\gamma}_k^{(i)}. \tag{31}$$

According to the principle of the chi-square test, when the null hypothesis is true, the test statistic $q_k^{(i)}$ should follow a central chi-square distribution with the corresponding degree of freedom. While when the alternative hypothesis is true, the test statistic $q_k^{(i)}$ follows a non-central chi-square distribution with the corresponding degree of freedom and a noncentrality

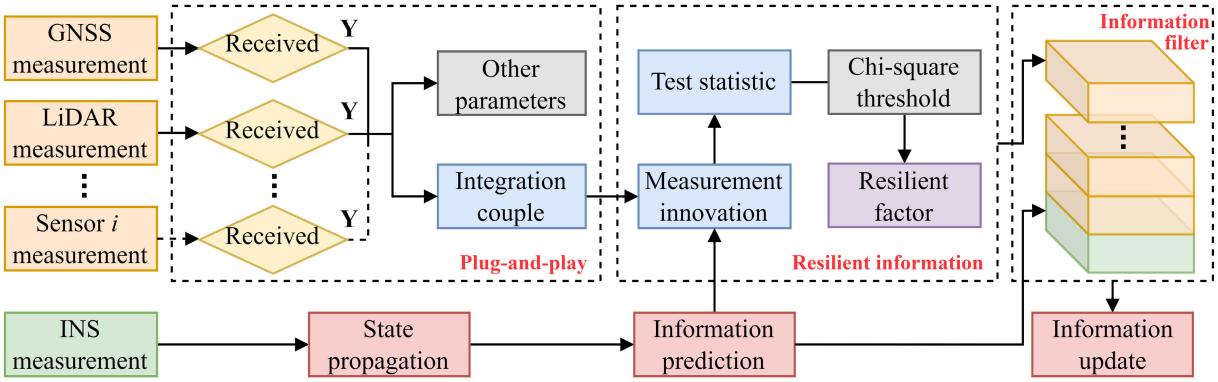

Fig. 3. Solution framework of the proposed plug-and-play navigation method.

parameter. Then the computed value of the test statistic will increase. Therefore, if the false alarm probability is given, the probability of the null hypothesis being true is

$$P\left(q_k^{(i)} \le \chi^2(1-\alpha, \text{dof})\right) = 1-\alpha \tag{32}$$

where $\chi^2(1-\alpha, \text{dof})$ is the chi-square value with the false alarm probability α and the degree of freedom dof.

When (32) holds, the ith sensor is considered fault-free, and its information is fully utilized in the integration process of IF. However, when this equation does not hold, the ith sensor is no longer reliable and it is necessary to exclude it from the system.

In this article, due to the application of plug-and-play navigation, there are many periods when the filter is performed using a single sensor. In this case, if this single sensor is consistently excluded, only the INS will work, which may lead to a continuous accumulation of errors. Thus, this article considers retaining the reliable information of the sensor as much as possible for integration. Then the resilient factor can be calculated as

$$\lambda_k^{(i)} = \begin{cases} 1, & q_k^{(i)} \le \chi^2(1-\alpha, \text{dof}) \\ \chi^2(1-\alpha, \text{dof}) \Big/ q_k^{(i)}, & q_k^{(i)} > \chi^2(1-\alpha, \text{dof}). \end{cases} \tag{33}$$

Finally, the solution framework of the proposed plug-and-play navigation method based on resilient IF is given in Fig. 3. Besides the sensors used in this article, the framework extends the system to the ith sensor, meeting the requirements of multisensor integration.

1) Plug-and-play box receives sensor measurements at each epoch and integrates them with different couples, maximizing the use of asynchronous information. Then other parameters such as propagation interval and system noise covariance will be adapted based on actual physical significance, which is discussed in the following experiment.
2) The resilient information box calculates the test statistic of each sensor measurement. Then resilient factor can be evaluated to adjust sensor information dynamically online with the selected chi-square threshold.
3) IF functions as a "building block." The prior information predicted from INS measurement acts as the green foundation and the resilient sensor information is added on top, much like stacking building blocks. The information is subsequently updated, producing a reliable navigation solution.

TABLE I
TYPES AND SAMPLE FREQUENCY OF NAVIGATION SENSORS

Sensor	Type	Sample frequency
IMU	Xsens MTi-10	100Hz
GNSS	Ublox M8T	1Hz
LiDAR	Velodyne HDL 32E	10Hz

IV. EXPERIMENT RESULTS AND ANALYSIS

To evaluate the effectiveness and resilience of the proposed resilient plug-and-play navigation method, vehicle experiments and analysis in an urban canyon environment are conducted in this section. The data collection of the vehicle dataset is introduced first, and then the positioning errors and accuracy are computed and compared between different methods.

A. Data Collection

The data collected for the experiment is a vehicle open-source dataset provided by the Intelligent Positioning and Navigation Laboratory (IPNL), Hong Kong Polytechnic University [41]. The system utilizes INS, GNSS, and LiDAR. All of the sensors are installed on the top of the experimental vehicle, which is shown in Fig. 4. The details of the sensors are shown in Table I.

This dataset was collected in East Tsim Sha Tsui, Hong Kong, where tall and densely packed buildings create a typical urban canyon environment. The trajectory of the dataset can be seen in Fig. 5. The operational trajectory in the real urban scenario is given in Fig. 5(a), and the positioning trajectory of each navigation sensor in the East-North (EN) coordinate is shown in Fig. 5(b). Among them, the reference trajectory is provided by Novatel SPAN-CPT, which is a GNSS/INS-integrated navigation system widely used for accurate positioning results. The GNSS solution is calculated by

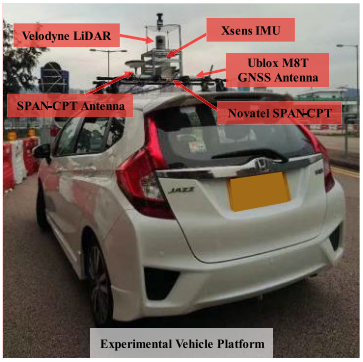

Fig. 4. Experimental vehicle platform for data collection [41].

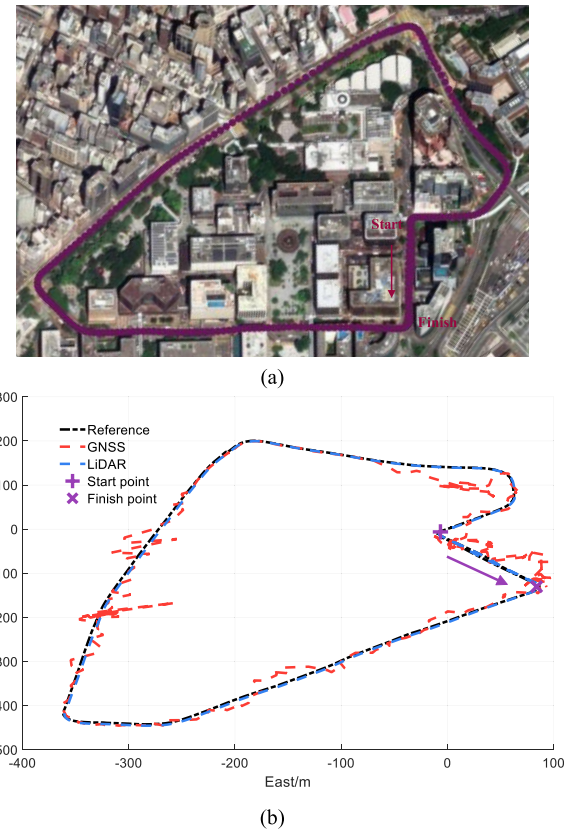

Fig. 5. Trajectory of the INS/GNSS/LiDAR dataset. (a) Trajectory in the real urban scenario. (b) Reference and positioning trajectory of each navigation sensor in EN coordinate.

the single point positioning (SPP) and the LiDAR solution is obtained by the point registration algorithm normal distribution transformation (NDT) in this experiment [42]. It is obvious that there are significant errors in the GNSS solution, resulting in low positioning accuracy. In contrast, the LiDAR solution has higher precision and can provide reliable positioning results in most cases.

B. Plug-and-Play Navigation Experiment

This experiment compares the positioning performance between KF, IF, and plug-and-play IF (PIF). Due to the problems of sampling delays and time desynchronization of the sensors, both KF and IF use GNSS sampling points as a reference, aligning the time of LiDAR for integration. To facilitate the sensor time alignment for PIF, this article considers preprocessing and interpolating the sensor time to the nearest level 10^{-1}. Fig. 6 and Table II show the positioning errors of KF, IF, and PIF in East-North-Up (ENU) coordinate.

TABLE II
RMS ERRORS OF THREE METHODS (KF, IF, AND PIF)

Item	KF	IF	PIF
E/m	2.46	2.46	1.65
N/m	3.66	3.66	2.02
U/m	8.00	8.00	3.59
3-D/m	9.13	9.13	4.44

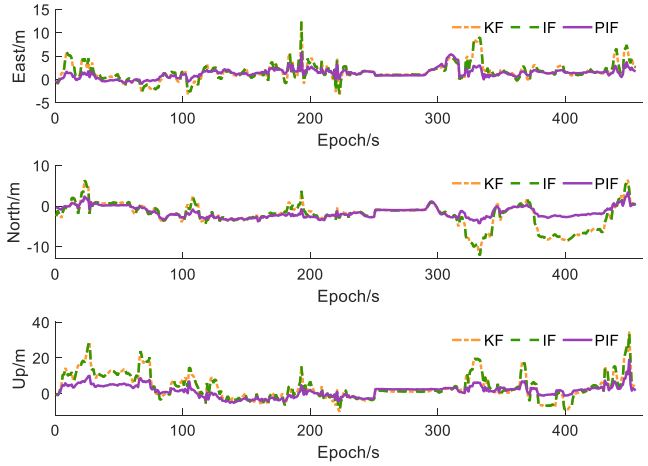

Fig. 6. Positioning errors of three methods (KF, IF, and PIF) in ENU coordinate.

It can be seen that KF and IF have the same positioning performance, with the 3-D root mean square (rms) errors of 9.13 m. Therefore, in agreement with the derivation in Section III, KF and IF are equivalent and they differ only in the form of the solution. Then, KF/IF is used to represent the two methods in following experiments.

To realize the multisensor integration, the system uses 486 couples of GNSS and LiDAR measurements in KF with a propagation interval of about 1 s. As a result, abundant LiDAR measurements are wasted between this interval. As described in this article, the system can easily achieve the ability of plug-and-play based on IF, which is shown as the PIF. As more valid LiDAR measurements enter the solving process, it is clear that PIF significantly improves the positioning results. From the 3-D perspective, PIF can reduce the error to 4.44 m, with a 51.37% improvement over KF and IF. However, the period around epoch 300 in Fig. 6 shows that PIF's positioning error is slightly greater than that of KF and IF, which means when less accurate measurements are used, the positioning accuracy of PIF will also decline.

C. Effect of Resilient Plug-and-Play Navigation Method

After the application of plug-and-play navigation, the system can calculate the corresponding resilient factor for each sensor in PIF, with the false alarm probability set to 10^{-3}.

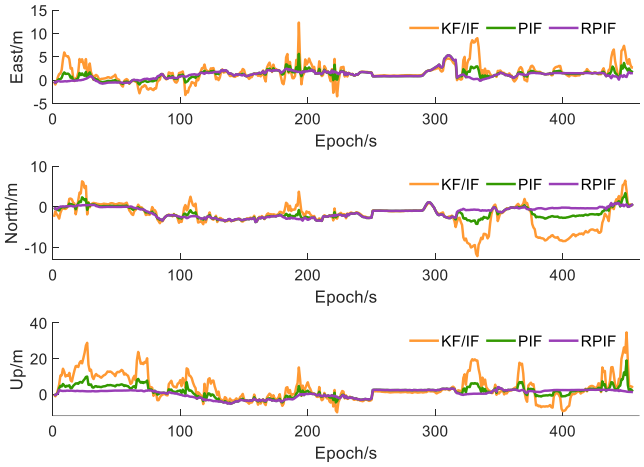

(a)

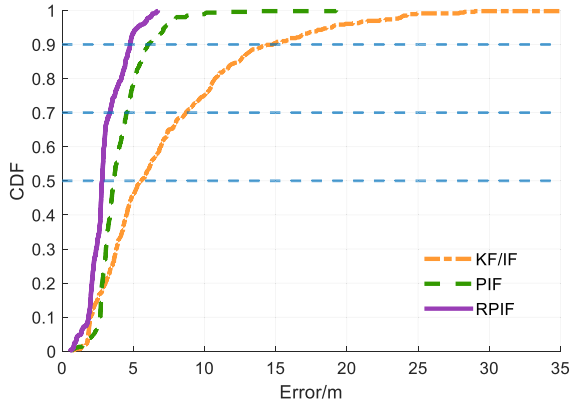

(b)

Fig. 7. Positioning errors of three methods (KF/IF, PIF, and RPIF). (a) Positioning errors in ENU coordinate. (b) CDF of 3-D positioning errors.

The positioning errors of KF/IF, PIF, and RPIF are shown in Fig. 7. From the ENU coordinate positioning errors in Fig. 7(a), it is shown that RPIF can further improve the positioning accuracy compared to PIF after adjusting the weight of sensor information, especially when the resilient factor is close to 0 in the faulty periods. It can also be seen that the errors of RPIF around epoch 300 are consistent with that of PIF. Combined with the calculated resilient factor, the additional data at this period are not accurate enough but within the chi-square threshold. Therefore, the weight of less-accurate measurements discussed in the last part will not be adjusted in RPIF, keeping the slighter rise in the positioning error. Fig. 7(b) represents the cumulative distribution function (cdf) of 3-D errors which can display the distribution of them directly. It is evident in the figure that when the cumulative probability is fixed, the proposed method has higher accuracy, and when a specific error is chosen, the availability of the proposed method is also better.

Then the 3-D rms error, mean error, and cdf of error under different cumulative probabilities of the three methods are given in Table III. In comparison with the rms error of KF/IF and PIF, the 3-D rms error of RPIF can be reduced to 3.28 m,

TABLE III
3-D POSITIONING ERRORS (RMS ERROR, MEAN ERROR, AND CDF) OF THREE METHODS (KF/IF, PIF, AND RPIF)

Item	KF/IF	PIF	RPIF
RMS error	9.13	4.44	3.28
Mean error	7.30	4.08	3.05
50% CDF	5.58	3.66	2.83
70% CDF	8.72	4.53	3.36
90% CDF	14.81	6.03	4.78

with a 64.07% accuracy improvement over KF and IF, and a 26.13% accuracy improvement over PIF, which proves that the navigation method proposed in this article is generally more advantageous. Meanwhile, the mean error can also verify the effectiveness of the proposed method. Comparing the 50% cdf, 70% cdf, and 90% cdf of the error separately, it can be seen that the proposed method can exhibit the best positioning performance consistently.

V. DISCUSSION

The comparison of innovations between KF/IF and PIF of each sensor is shown in Fig. 8. Here the innovations represent the difference between measurements and predictions, as calculated in (29).

Fig. 8(a) compares the three-axis innovations of GNSS measurement. Combined with Fig. 6, it can be seen that during the segments with large errors, the absolute value of the innovations of PIF is significantly greater than that of the KF/IF. This can be attributed to that when the measurement values remain unchanged, the predicted values are continuously corrected by the LiDAR measurements, as a result of which, the difference between the measurements and predictions has increased.

Similarly, Fig. 8(b) compares the three-axis innovations of LiDAR measurement. On one hand, the innovation value of LiDAR is significantly lower than that of GNSS in most cases. This indicates that the GNSS sensor receiver is easily affected by NLOS in urban canyon environments, leading to its measurements being unreliable. On the other hand, the innovation value of KF/IF is greater than that of PIF, especially in faulty periods. Due to the application of plug-and-play navigation, the position estimation is continuously refined by additional measurements, bringing it closer to the LiDAR measurement. Therefore, the positioning errors are constantly corrected and the LiDAR measurement is more reliable than the GNSS measurement. Additionally, the small images in Fig. 8(b) are the enlargement of PIF's innovations from epoch 325 to epoch 340. It can be seen that the innovation value will increase when a couple of GNSS and LiDAR measurements are applied to the filter. Then the innovation value gradually decreases with the detection and application of the LiDAR measurements.

Apart from the points discussed above, another influential factor is the propagation interval. Unlike the traditional filter, the interval in plug-and-play navigation is shorter, which is about 0.1 s in this article. Consequently, the calculation of the system noise covariance will also be reduced. There is no doubt that when the interval and covariance are larger, the system tends to trust the measurements more, while when the

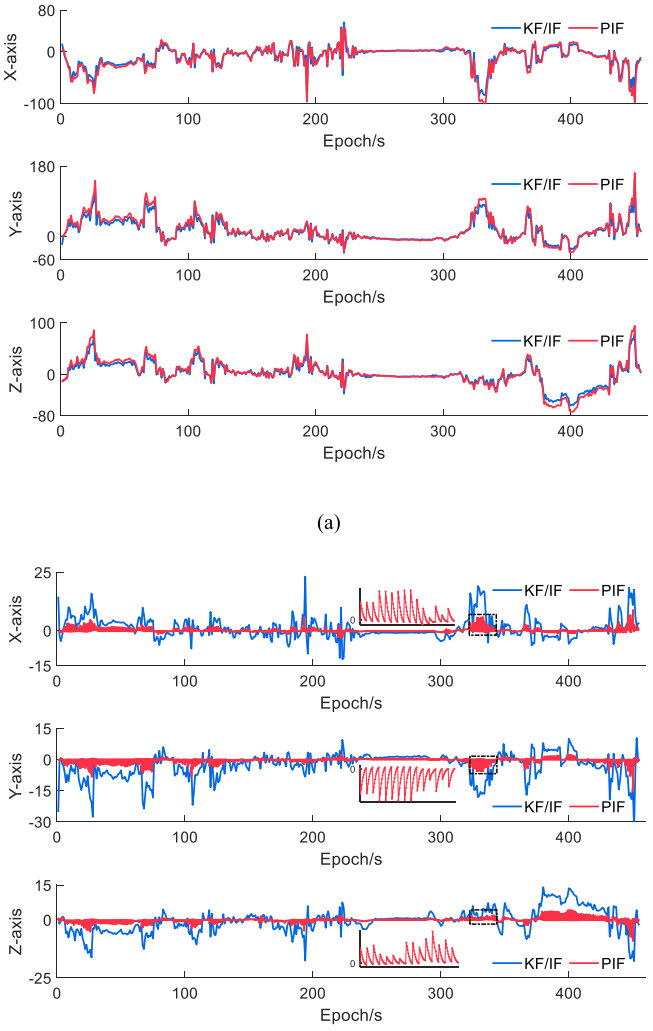

Fig. 8. Innovations comparison between KF/IF and PIF of each sensor. (a) Three-axis innovations of GNSS measurements. (b) Three-axis innovations of LiDAR measurements.

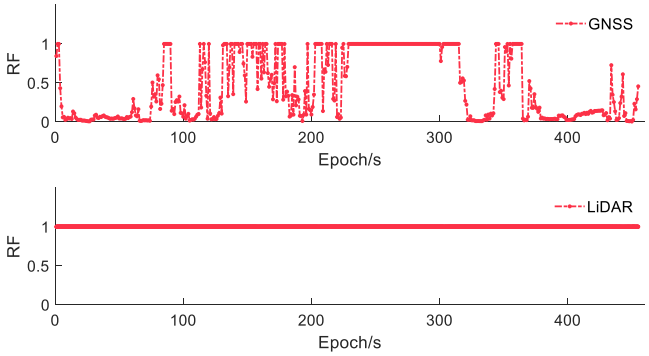

Fig. 9. Resilient factor of GNSS and LiDAR measurements.

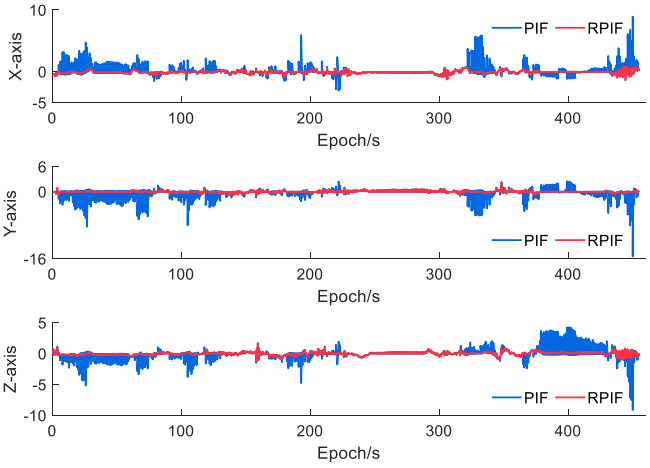

Fig. 10. Three-axis innovations comparison between PIF and RPIF of LiDAR measurements.

interval and covariance are smaller, the system relies more on the predictions. Therefore, it can be seen in the small images in Fig. 8(b), that although the same measurements are applied to the system, their impact on positioning estimation is not as significant as that in KF/IF. From this point, it can be indicated that a smaller propagation interval provides better robustness to the measurements, especially against outliers and faults. Meanwhile, a smaller interval also implies more measurements, which continuously correct the positioning results. Therefore, the sensitivity of PIF to sensor measurement noise and faults is much lower than that of traditional KF.

The resilient factor of GNSS and LiDAR are shown in Fig. 9. The test statistic for LiDAR is always below the chi-square threshold, so the resilient factor for it has constantly been 1, which means that the LiDAR measurements are reliable with the selected false alarm probability. However, the test statistic for GNSS is above the threshold in most epochs, causing the resilient factor to fluctuate between 0 and 1 continuously. Therefore, sensor information of GNSS will be adjusted before being incorporated into the IF in RPIF. Moreover, Fig. 9 can further explain the advantage of PIF over KF and IF, for that the additional measurements used by PIF come mainly from high-frequency LiDAR sensors. In most cases, they are generally more reliable than those of GNSS, allowing PIF to significantly improve the positioning performance.

As shown in Fig. 10, the three-axis innovations of LiDAR measurement are compared. As a result of the adjustment of sensor information by the resilient factor, it is evident from the figure that the LiDAR innovation value of the RPIF is smaller than that of the PIF. When the system detects GNSS measurements and performs filtering, the influence on position estimation is further reduced due to the suppression of faults in Fig. 9. Similarly, in the period where the resilient factor of GNSS is 1, the innovations of the two methods are essentially coincident. Therefore, the resilient factor can directly address the faulty sensor based on PIF, further enhancing the resilience of the navigation system in this article.

VI. Conclusion

To improve the accuracy and robustness of the multisensor integration, a resilient plug-and-play navigation method

based on IF is proposed in this article. Compared to the traditional KF, the proposed method can achieve asynchronous information fusion and plug-and-play navigation flexibly. With more measurements and smaller propagation intervals, this method can continuously refine the positioning results and maintain robustness against outliers. The impact of faulty measurements can be further reduced by introducing a resilient factor based on the principle of the chi-square test to adjust the sensor information, effectively improving the resilience and continuity of the system.

The open-sourced INS/GNSS/LiDAR vehicle experiments in urban canyon environments are conducted to verify the effectiveness of the proposed method. The equivalence of KF and IF has been validated. Then, the reasons that PIF and RPIF can progressively improve positioning performance are analyzed from the perspective of sensor innovation. The former method can reduce the system's sensitivity to faults, and the latter method directly addresses the faults themselves. Both cdf and ENU coordinates of errors demonstrate that the proposed method can achieve resilient navigation in challenging environments.

As discussed above, although IF has been implemented, this article still utilizes the chi-square test in the state domain to calculate the resilient factor. Therefore, future work will focus on researching characteristics of information parameters and studying FDE algorithms based on the information domain. Then, different sensors such as vision and odometer will be introduced to verify the superiority of plug-and-play navigation based on resilient IF. Additionally, other integration methods like interactive multiple models will also be considered for application in the existing multisensor system.

REFERENCES

[1] S. Bijjahalli and R. Sabatini, "A high-integrity and low-cost navigation system for autonomous vehicles," *IEEE Trans. Intell. Transp. Syst.*, vol. 22, no. 1, pp. 356–369, Jan. 2021.

[2] B. Gong, S. Wang, M. Hao, X. Guan, and S. Li, "Range-based collaborative relative navigation for multiple unmanned aerial vehicles using consensus extended Kalman filter," *Aerosp. Sci. Technol.*, vol. 112, May 2021, Art. no. 106647.

[3] F. Zangenehnejad and Y. Gao, "GNSS smartphones positioning: Advances, challenges, opportunities, and future perspectives," *Satell. Navigat.*, vol. 2, no. 1, p. 24, Nov. 2021.

[4] Z. Yang, H. Zhao, and X. Yang, "A novel navigation method fusing multiple constraint for low-cost INS/GNSS integrated system in urban environments," *IEEE Trans. Veh. Technol.*, vol. 73, no. 6, pp. 7616–7629, Jun. 2024.

[5] Y. Ding, P. Chauchat, G. Pages, and P. Asseman, "Learning-enhanced adaptive robust GNSS navigation in challenging environments," *IEEE Robot. Autom. Lett.*, vol. 7, no. 4, pp. 9905–9912, Oct. 2022.

[6] K. Chiang, Y. Chiu, S. Srinara, and M. Tsai, "Performance of LiDAR-SLAM-based PNT with initial poses based on NDT scan matching algorithm," *Satell. Navigat.*, vol. 4, no. 1, p. 3, Dec. 2023.

[7] Q. Meng and L. Hsu, "Resilient interactive sensor-independent-update fusion navigation method," *IEEE Trans. Intell. Transp. Syst.*, vol. 23, no. 9, pp. 16433–16447, Sep. 2022.

[8] Z. Fan and L. Zhao, "Autonomous integrity of multisource information resilient fusion navigation system: State-of-the-art and open challenges," *IEEE Trans. Instrum. Meas.*, vol. 73, pp. 1–17, 2024.

[9] Q. Meng, Y. Song, S.-Y. Li, and Y. Zhuang, "Resilient tightly coupled INS/UWB integration method for indoor UAV navigation under challenging scenarios," *Defence Technol.*, vol. 22, pp. 185–196, Apr. 2023.

[10] F. Wu, H. Luo, H. Jia, F. Zhao, Y. Xiao, and X. Gao, "Predicting the noise covariance with a multitask learning model for Kalman filter-based GNSS/INS integrated navigation," *IEEE Trans. Instrum. Meas.*, vol. 70, pp. 1–13, 2021.

[11] J. Zhang, W. Wen, F. Huang, X. Chen, and L.-T. Hsu, "Coarse-to-fine loosely-coupled LiDAR-inertial odometry for urban positioning and mapping," *Remote Sens.*, vol. 13, no. 12, p. 2371, Jun. 2021.

[12] Y. X. Yang, "Resilient PNT concept frame," *Acta Geod. et Cartogr. Sin.*, vol. 47, no. 7, pp. 893–898, 2018.

[13] W. Wang, W. Shangguan, J. Liu, and J. Chen, "Enhanced fault detection for GNSS/INS integration using maximum correntropy filter and local outlier factor," *IEEE Trans. Intell. Vehicles*, vol. 9, no. 1, pp. 2077–2093, Jan. 2024.

[14] Q. Meng and L.-T. Hsu, "Integrity monitoring for all-source navigation enhanced by Kalman filter-based solution separation," *IEEE Sensors J.*, vol. 21, no. 14, pp. 15469–15484, Jul. 2021.

[15] J. Xiong, J. W. Cheong, Z. Xiong, A. G. Dempster, S. Tian, and R. Wang, "Adaptive hybrid robust filter for multi-sensor relative navigation system," *IEEE Trans. Intell. Transp. Syst.*, vol. 23, no. 8, pp. 11026–11040, Aug. 2022.

[16] Y. Jiang et al., "Robust Kalman filter enhanced by projection statistic detector for multisensor navigation in urban canyon environment," *IEEE Sensors J.*, vol. 23, no. 9, pp. 9832–9847, May 2023.

[17] S. Hewitson and J. Wang, "Extended receiver autonomous integrity monitoring (eRAIM) for GNSS/INS integration," *J. Surveying Eng.*, vol. 136, no. 1, pp. 13–22, Feb. 2010.

[18] R. Duchnowski and P. Wyszkowska, "Robust procedures in processing measurements in geodesy and surveying: A review," *Meas. Sci. Technol.*, vol. 35, no. 5, May 2024, Art. no. 052002.

[19] J. Zhou, "Classical theory of errors and robust estimation," *Acta Geod. et Cartogr. Sin.*, no. 2, pp. 115–120, 1989.

[20] Y. Yang, L. Song, and T. Xu, "Robust parameter estimation for geodetic correlated observations," *Acta Geod. et Cartogr. Sin.*, vol. 31, no. 2, pp. 95–99, 2002.

[21] R. Chen and L. Zhao, "Multi-level autonomous integrity monitoring method for multi-source PNT resilient fusion navigation," *Satell. Navigat.*, vol. 4, no. 1, p. 21, Dec. 2023.

[22] H. Zhang, H. Xiong, S. Hao, G. Yang, M. Wang, and Q. Chen, "A novel multidimensional hybrid position compensation method for INS/GPS integrated navigation systems during GPS outages," *IEEE Sensors J.*, vol. 24, no. 1, pp. 962–974, Jan. 2024.

[23] J. S. Gipson and R. C. Leishman, "A framework for collaborative all-source navigation with fault detection and exclusion," *IEEE Trans. Aerosp. Electron. Syst.*, vol. 58, no. 5, pp. 4615–4625, Oct. 2022.

[24] J. D. Jurado and J. F. Raquet, "Autonomous and resilient management of all-source sensors," in *Proc. ION Pacific PNT Meeting*, Honolulu, HI, USA, May 2019, pp. 142–159.

[25] H. Xiong, R. Bian, Y. Li, Z. Du, and Z. Mai, "Fault-tolerant GNSS/SINS/DVL/CNS integrated navigation and positioning mechanism based on adaptive information sharing factors," *IEEE Syst. J.*, vol. 14, no. 3, pp. 3744–3754, Sep. 2020.

[26] G. Hu, L. Xu, B. Gao, L. Chang, and Y. Zhong, "Robust unscented Kalman filter-based decentralized multisensor information fusion for INS/GNSS/CNS integration in hypersonic vehicle navigation," *IEEE Trans. Instrum. Meas.*, vol. 72, pp. 1–11, 2023.

[27] S. Bai, J. Lai, P. Lv, Y. Cen, B. Wang, and K. Huang, "Multisensory plug-and-play factor graph fusion method based on IMU/odometer preintegration," *J. Chin. Inertial Technol.*, vol. 28, no. 5, pp. 624–628&637, 2020.

[28] Z. Li, Q. Meng, Z. Shen, L. Wang, L. Li, and H. Jia, "Resilient factor graph-based GNSS/IMU/vision/odo integrated navigation scheme enhanced by noise approximate Gaussian estimation in challenging environments," *Remote Sens.*, vol. 16, no. 12, p. 2176, Jun. 2024.

[29] H. Dai, H. Bian, H. Ma, and R. Wang, "Application of robust incremental smoothing algorithm based on factor graph in integrated navigation of unmanned surface vehicle," *J. Chin. Inertial Technol.*, vol. 26, no. 6, pp. 778–786, 2018.

[30] X. Wu, B. Xiao, C. Wu, Y. Guo, and L. Li, "Factor graph based navigation and positioning for control system design: A review," *Chin. J. Aeronaut.*, vol. 35, no. 5, pp. 25–39, May 2022.

[31] N. Assimakis, M. Adam, and A. Douladiris, "Information filter and Kalman filter comparison: Selection of the faster filter," *Int. J. Inf. Eng.*, vol. 2, pp. 1–5, Mar. 2012.

[32] S. Thrun, W. Burgard, and D. Fox, "Gaussian filters," in *Probabilistic Robotics*. Cambridge, MA, USA: MIT Press, 2006, pp. 71–75.

[33] P. D. Groves, "System model and state selection," in *Principles of GNSS, Inertial, and Multisensor Integrated Navigation Systems*, 2nd ed., Norwood, MA, USA: Artech House, 2013, p. 584.

[34] Y. Qin, H. Zhang, and S. Wang, "Discrete Kalman filter," in *Kalman Filter and Integrated Navigation Principle*, 3rd ed., Xian, China: Northwestern Polytechnical Univ. Press, 2015, pp. 42–43.
[35] J. R. Raol, "Concepts and theory of data fusion," in *Multi-Sensor Data Fusion With MATLAB*, 1st ed., Boca Raton, FL, USA: CRC Press, 2009, pp. 34–36.
[36] B. Siciliano and O. Khatib, "Multisensor data fusion methods," in *Springer Handbook of Robotics*, 2nd ed., Berlin, Germany: Springer, 2016, pp. 868–876.
[37] W. Pan, X. Zhan, and X. Zhang, "Fault exclusion method for ARAIM based on tight GNSS/INS integration to achieve CAT-I approach," *IET Radar, Sonar Navigat.*, vol. 13, no. 11, pp. 1909–1917, Nov. 2019.
[38] J. D. Jurado and J. F. Raquet, "Towards an online sensor model validation and estimation framework," in *Proc. IEEE/ION Position, Location Navigat. Symp. (PLANS)*, Monterey, CA, USA, Apr. 2018, pp. 1319–1325.
[39] J. Al Hage, P. Xu, P. Bonnifait, and J. Ibanez-Guzman, "Localization integrity for intelligent vehicles through fault detection and position error characterization," *IEEE Trans. Intell. Transp. Syst.*, vol. 23, no. 4, pp. 2978–2990, Apr. 2022.
[40] L. Wang, K. Zhi, B. Li, and Y. Zhang, "Dynamically adjusting filter gain method for suppressing GNSS observation outliers in integrated navigation," *J. Navigat.*, vol. 71, no. 6, pp. 1396–1412, Nov. 2018.
[41] L.-T. Hsu et al., "Hong Kong UrbanNav: An open-source multisensory dataset for benchmarking urban navigation algorithms," *Navig., J. Inst. Navigat.*, vol. 70, no. 4, pp. 1–29, Dec. 2023.
[42] W. Wen, L.-T. Hsu, and G. Zhang, "Performance analysis of NDT-based graph SLAM for autonomous vehicle in diverse typical driving scenarios of Hong Kong," *Sensors*, vol. 18, no. 11, p. 3928, Nov. 2018.

Qian Meng (Member, IEEE) received the B.Eng. degree in automation and the Ph.D. degree in control science and engineering from Nanjing University of Aeronautics and Astronautics, Nanjing, China, in 2013 and 2018, respectively.

He was a Visiting Ph.D. Student at the Center of Transport Studies, Imperial College London, London, U.K., in 2017. He was a Postdoctoral Fellow with the Department of Aeronautical and Aviation Engineering, Hong Kong Polytechnic University, Hong Kong, from 2019 to 2021. He is currently an Associate Professor at Southeast University, Nanjing. His current research interests focus on resilient and reliable navigation and positioning, integrity for global navigation satellite system (GNSS), multisensor integration, and GNSS receiver signal processing.

Dr. Meng is a member of ION. He serves as a member on the editorial board and a reviewer in professional journals related to navigation and positioning.

Chang Su received the B.Eng. degree from Southeast University, Nanjing, China, in 2023, where he is pursuing the master's degree with the School of Instrument Science and Engineering.

His current research interests focus on inertial navigation system (INS)/global navigation satellite system (GNSS) integrated navigation, multisensor integrated navigation, and its reliable positioning.

Yingying Jiang (Graduate Student Member, IEEE) received the B.Sc. degree from Anhui University of Science and Technology, Huainan, China, in 2019, and the M.Sc. degree from Southeast University, Nanjing, China, in 2023. She is pursuing the Ph.D. degree with the GEOLOC Laboratory, Gustave Eiffel University, Nantes, France.

Her main research interests focus on fault detection and exclusion of global navigation satellite system (GNSS)/inertial navigation system (INS)-integrated positioning, multisensor integration, and its integrity.

Weisong Wen (Member, IEEE) received the B.Eng. degree in mechanical engineering from Beijing Information Science and Technology University, Beijing, China, in 2015, the M.Eng. degree in mechanical engineering from China Agricultural University, Beijing, in 2017, and the Ph.D. degree in mechanical engineering from Hong Kong Polytechnic University (PolyU), Hong Kong, in 2020.

He was a Visiting Ph.D. Student with the Faculty of Engineering, University of California at Berkeley, Berkeley, CA, USA, in 2018. He was a Research Assistant Professor at AAE, PolyU, since 2021. He was an Assistant Professor at PolyU in 2023. He has published 30 SCI articles and 40 conference papers in the field of GNSS (ION GNSS+) and navigation for robotic systems (IEEE ICRA and IEEE ITSC), such as autonomous driving vehicles.

Xiaolin Meng is the Chair Professor of Intelligent Mobility with the School of Instrument Science and Engineering, Southeast University, Nanjing, China. He was a Professor of Intelligent Mobility and the Theme Leader of Positioning and Navigation Technologies, University of Nottingham, Nottingham, U.K., until May 2020. He has authored more than 380 publications and undertaken a research portfolio of more than £18m. His research interests mainly include intelligent transportation systems and smart cities, connected and autonomous vehicles, structural health monitoring of large infrastructure, and precision agriculture/livestock farming.